# Atomic-level study of $BiFeO_3$ under epitaxial strain

M. Graf, M. Sepliarsky,* and M. G. Stachiotti
*Instituto de Física Rosario, Consejo Nacional de Investigaciones Científicas y Técnicas (CONICET) and Universidad Nacional de Rosario, Rosario, Argentina*
(Received 9 May 2016; published 1 August 2016)

Structural and thermal properties of $BiFeO_3$ under compressive epitaxial strain are investigated using a shell model fitted to first-principles calculations. We show that a model developed for the bulk describes properly the behavior of the compound as function of the strain, including the appearance of tetragonallike phase with a large $c/a$ ratio. The obtained temperature-strain phase diagram reproduces several features observed experimentally in thin films. Molecular dynamic simulations show that morphotropic phase boundary separating the $R$-like and $T$-like regions is temperature independent but with different phases along the transition region. The microscopic analysis of the temperature-strain phase diagram emphasizes the relevance of the interplay between polarization, oxygen octahedron rotations, and strain.

DOI: 10.1103/PhysRevB.94.054101

## I. INTRODUCTION

The perovskite $BiFeO_3$ (BFO) is distinguished by its unique properties and potential applications. The BFO is the prototypical single compound to understand multiferroic behavior since it displays simultaneously ferroelectric and magnetic properties at room temperature [1–3]. In addition, this material is also under consideration as a lead-free compound for ferroelectric and piezoelectric applications due to its large spontaneous polarization ($P_s = 100\,\mu C\,cm^{-2}$) and high Curie temperature ($T_C = 1083\,K$). As in many other pure perovskite ferroelectrics, the room temperature piezoelectric coefficients of BFO are rather small [4–7], but the structure can be engineered to enhance its properties. Values of piezoelectric coefficients comparable to those of the conventional $PbTi_xZr_{1-x}O_3$ (PZT) have been reported in BFO-based solid solutions [8,9] as well as in strained epitaxial films [10], making the system suitable for high-performance piezoelectric applications for ecofriendly devices [11]. In fact, the discovery of a strain-stabilized supertetragonal phase with a giant $c/a$ ratio has triggered an intense research activity due to both fundamental interest and the technological importance.

When BFO is epitaxially grown as a thin film onto a compressive substrate, unexpected results have been observed. Under moderate levels of compressive strains, for instance, an anomalous decrease of $T_C$ with compressive strains has been found, which is in contrast to what is commonly observed in classical ferroelectrics [12,13]. Larger strains induce the abrupt elongation of the out-of-plane lattice parameter and a strong increment of the polarization. This polymorphic transition is also named as a morphotropic phase boundary (MPB) since it resembles the behavior of the one observed in lead-based ferroelectrics solid solution like PZT or $PbMg_{1/3}Nb_{2/3}O_3$-$PbTiO_3$ (PMN-PT) [10]. While the large piezoelectric response near the MPB is attributed to coexistence of phases in this region, the structural evolution path as function of the strain and temperature are still under debate. Structures of various symmetries and different sequences of phase transitions have been reported (see Ref. [14] for a review).

The peculiar behavior of BFO is related with a complex energy landscape, where a wide variety of metastable phases, very close in energy, are present [15,16]. The BFO is a highly distorted perovskite, with the structure dominated by the off-centering displacements of Bi cations and the rotation of the oxygen octahedra. The ground state is rhombohedral of $R3c$ symmetry with two formula units per unit cell, a ferroelectric polarization along the [111] pseudocubic direction [17], and an antiphase tilting of oxygen octahedral rotations along the same direction, $a^-a^-a^-$ in terms of Glazer notation. At $T_C$, the compound undergoes a first-order transition to an orthorhombic phase of *Pbnm* symmetry (formally *Pnma*) with four formula units per unit cell and is characterized by antiphase oxygen rotations around [110] and in-phase rotations around [001] [18]. This phase is considered as paraelectric, even though signals related to an antiferroelectric order have been suggested [16,19–21]. The structural behavior of BFO is very sensitive to deformation, and the way that strain modifies the strength of the instabilities is an issue of significant relevance for understanding of the functional properties of the compound.

In this paper, we study the effects of the epitaxial strain imposed by cubic substrates on the structural properties of BFO by using an atomic-level approach. The model was obtained from first-principles calculations, and it was recently used to describe bulk properties, including the phase diagram, and dielectric and piezoelectric responses as function of temperature [7,21].

## II. MODEL AND COMPUTATIONAL DETAILS

The shell model has been extensively used to study finite temperature properties in ferroelectric compounds [22–25]. In this approach, each atom is described as two charged and coupled particles: a core and a shell. The model includes electrostatic interactions among cores and shells of different atoms and short-range interactions between shells. The model potential of BFO used in this paper was fitted to reproduce first-principles results. Since the input data correspond to results obtained within the local density approximation (LDA+$U$), lattice parameters and related properties are underestimated with respect to experimental values. The model was able

*sepliarsky@ifir-conicet.gov.ar

 

to correctly reproduce the direct transition from the low-temperature $R3c$ ferroelectric phase to the *Pbnm* orthorhombic phase of the bulk, as well as microscopic characteristics of both phases [7,21].

We use this model to determine relaxed structures and finite temperature properties of BFO as a function of a compressive epitaxial strain. The strain, which is incorporated in the ferroelectric material due to the lattice mismatch with the substrate, is taken into account in the simulations by fixing the in-plane lattice parameters, while the length of the simulation cell in the $z$ direction was allowed to expand or contract to reach zero stress. The misfit strain is defined as $\varepsilon = (a - a_0)/a_0$, where $a$ is the imposed in-plane lattice parameter and $a_0$ is the pseudocubic lattice parameter of the unstrained $R3c$ phase obtained with the model. The molecular dynamic (MD) simulations were carried out with DL-POLY code [26] in a supercell size of $12 \times 12 \times 12$ 5-atom unit cells (8640 atoms) with periodic boundary conditions. The relaxed structures were determined as zero-temperature limit MD simulations. In order to avoid high-energy metastable states, successive heating and quenching were performed until the forces on individual ions were lower than $0.01\,\text{eV}\,\text{Å}^{-1}$. The runs were made at temperature intervals of 50 K and with a time step of 0.4 fs. Each MD run consists of at least 40 000 time steps for data collection after 20 000 time steps for thermalization.

## III. RESULTS AND DISCUSSION

### A. Zero-temperature evolution

We first investigate the relative stability of possible BFO structures as function of the misfit strain. Figure 1 shows the behavior of the energy for the relevant phases obtained with the model at zero temperature. The two-dimensional (2D) clamping imposed by the substrate breaks the symmetry of the bulk, and the obtained phases are distorted versions of the ones observed in bulk. The phases denoted as $R'$ and $O'$ correspond to distorted versions of the parent rhombohedral $R3c$ and orthorhombic *Pbnm* structures. We note that there are two possible *Pbnm*-distorted phases. In one of the structures, the in-phase rotation component is along the epitaxial direction, and the rotational order is represented as $(a^-a^-b^+)$. In the second one, the in-phase rotation component lies along one of the axes parallel to the substrate, i.e., the $y$ axis, and the order is represented as $(a^-b^+c^-)$. The structure referred here as $O'$ corresponds to the second configuration since it is energetically favorable. As it is observed in the figure, the $R'$ phase is the most stable at low levels of compressive strains, which is in concordance with theoretical and experimental evidence [27,28]. The energy of the $O'$ phase decreases until the in-plane lattice parameter reaches the value corresponding to the unstrained parent *Pbnm* structure. At that strain, the energies of $O'$ and $R'$ phases are very close, and both curves nearly overlap for strains larger than $-1.3\%$. While a *Pbnm* phase has been observed under hydrostatic [29] and chemical [9] pressure, there is no experimental evidence of the presence of an $O'$ type phase in strained films of pure BFO. This discrepancy may be related with the small energy difference between the parent structures and the complex energy behavior of BFO. In the model, the *Pbnm* phase is only $17\,\text{meV f.u.}^{-1}$ above the $R3c$ ground state, which is close to the LDA+$U$ value of $14\,\text{meV f.u.}^{-1}$ used to fit the model. We note that this energy difference is very sensitive to the election of exchange-correlation functional, and values up to $60\,\text{meV f.u.}^{-1}$ have been reported [15,16]. Despite the energy competition between the $R'$ and $O'$ phases, the model is able to account for the presence of the called supertetragonal ($T'$) phase, in agreement with experimental observations and theoretical results [10,27]. According to our model, the $T'$ structure becomes stable for misfit strains higher than $-3.7\%$, while the critical strain is $\sim -4.5\%$ in experiments [10], and first-principles values vary between $-2.3\%$ and $-4.5\%$ [16,30].

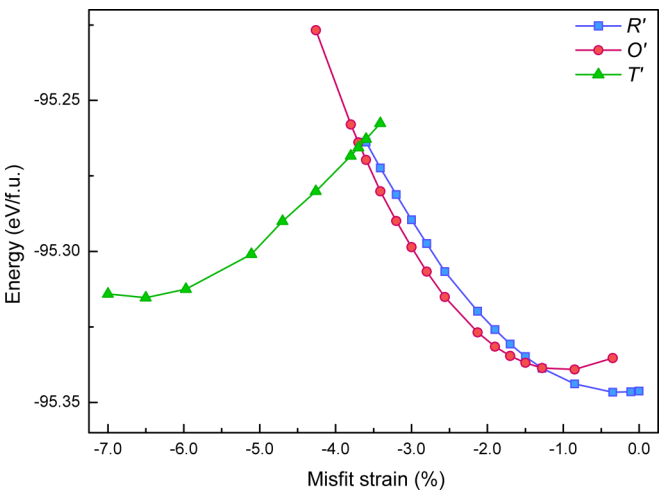


FIG. 1. Total energy as a function of the misfit strain for $R'$, $O'$, and $T'$ phases of $BiFeO_3$.

Now we analyze in more detail the structural behavior of the compound as a function of the epitaxial strain. We focus in the evolution from the $R'$ to the $T'$ phase. Figure 2 shows the significant magnitudes that characterize the structural behavior of the system: tetragonal distortion $c/a$ and in-plane stress (a), polarization $\boldsymbol{P}$ (b) and oxygen octahedron rotation patterns (c). As expected, $c/a$ increases, and $\boldsymbol{P}$ rotates toward the $z$ axis with the increment of the compressive strain. At $\varepsilon = -1.5\%$, which corresponds to a thin film deposited on $SrTiO_3$, the model gives $c/a = 1.04$ and $P_z = 48\,\mu\text{C cm}^{-2}$. These values are comparable with 1.04 and $58\,\mu\text{C cm}^{-2}$ obtained from LDA+$U$ calculations [31]. Concomitant with this, there is an enhancement of the antiphase oxygen-octahedra rotation angle around the epitaxial axis ($\omega_z$), while other components ($\omega_x$,$\omega_y$) decrease. As a result, the structure becomes monoclinic of $M_A$ type ($P_x = P_y < P_z$) with space group symmetry $Cc$. The transition to the $T'$ phase involves a sudden increase in $c/a$ and out-of-plane polarization. At the transition, $c/a$ increases from 1.09 to 1.22, while $P_z$ jumps from $63\,\mu\text{C cm}^{-2}$ to $100\,\mu\text{C cm}^{-2}$, values in close agreement with experiments and first-principles calculations [10,30]. The in-plane polar components are barely affected, but the in-plane stress condition changes from compressive to tensile. The strain-induced transition is also accompanied by a marked reduction in the values of the oxygen octahedra rotations, being the most pronounced the change along $z$ direction. Nevertheless, $\omega_z$ does not vanish, in contrast to first-principles results [30].

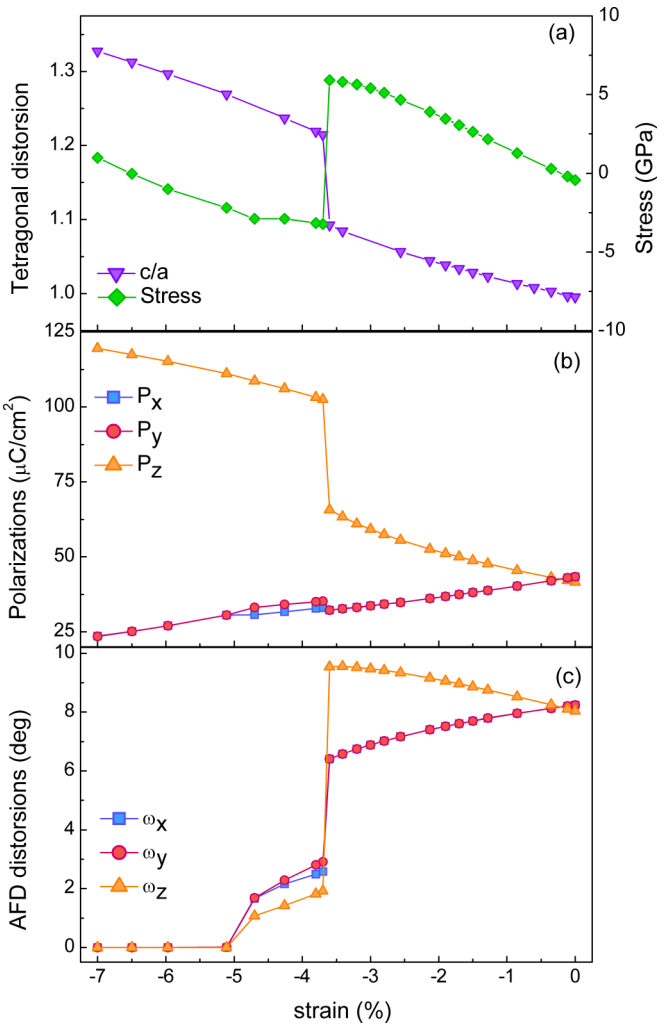


FIG. 2. Evolution of (a) tetragonal distortion and in-plane stress, (b) polarizations, and (c) antiphase oxygen octahedron rotations as a function of the misfit strain in $BiFeO_3$.

The symmetry of this $T'$ does not change at the transition. We denote as $T'(M_{A1})$ this $M_A$ phase with $C_C$ symmetry. The $T'(M_{A1})$ phase remains stable for strains up to $-5.1\%$, where a second transition is observed. In this polymorphic, the rotation of the oxygen octahedra completely vanishes, while the other magnitudes (energy, tetragonal distortion, and net polarization) do not display noticeable anomalies. However, an additional difference between the two $T'$ phases is observed in the in-plane local polarization pattern. While in the first phase, the local polarizations are slightly canted respect to the $[110]_{pc}$ direction forming a zigzag arrangement [Fig. 3(a)], the second phase displays the formation of a periodic domain structure with in-plane polarizations alternately pointing along $x$ and $y$ direction in a head-to-tail periodic arrangement [Fig. 3(b)]. In each domain, $\boldsymbol{P}$ is pointing alternatively along $[101]_{pc}$ and $[011]_{pc}$ directions. Each domain has a $M_C$ type of symmetry with space group $Pm$, and the structure is denoted as $T'(M_C)$. This configuration is consistent with periodic nanodomain patterns observed in BFO thin films grown on $LaAlO_3(\varepsilon = -4.8\%)$ [32].

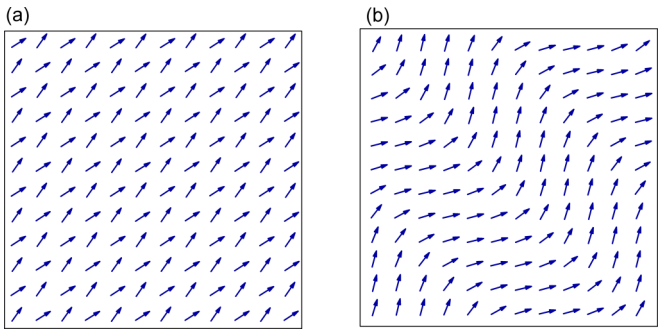


FIG. 3. In-plane local polarization pattern for the (a) $T'(M_{A1})$ and (b) $T'(M_C)$ structures at zero temperature.

The macroscopic evolution as a function of the compressive strain is microscopically connected with changes in the atomic positions. In fact, the abrupt changes in the tetragonal distortion and $P_z$ arise from large atomic displacements along $z$ direction, mainly of Bi and Fe atoms with respect to the oxygen. As shown in Fig. 4, Fe ions are shifted by 0.58 Å from the average $O_x - O_y$ plane, modifying the bond distance with $O_z$. In particular, the long bond displays an abrupt elongation, from 2.13 Å in the $R'$ phase to 2.78 Å in the $T'$ phase. The short bond, however, just experiments a small contraction, from 1.91 Å to 1.88 Å. In the case of Bi atoms, they move ∼0.95 Å toward one of the $O_x - O_y$ planes, forming two groups of Bi-O bonds, short and large. Model values of 2.31 Å and 3.82 Å are in agreement with experimental estimations of 2.33 Å and 3.78 Å, respectively [33].

### B. Strain-temperature phase diagram

The strain-temperature phase diagram of BFO obtained from the simulations is displayed in Fig. 5. The reported data do not include any kind of correction or rescaling. The epitaxial strain refers to the lattice parameters at 0 K. The phase diagram shows two markedly different zones corresponding to the bulk or $R$-like (right side) and tetragonal or $T$-like (left

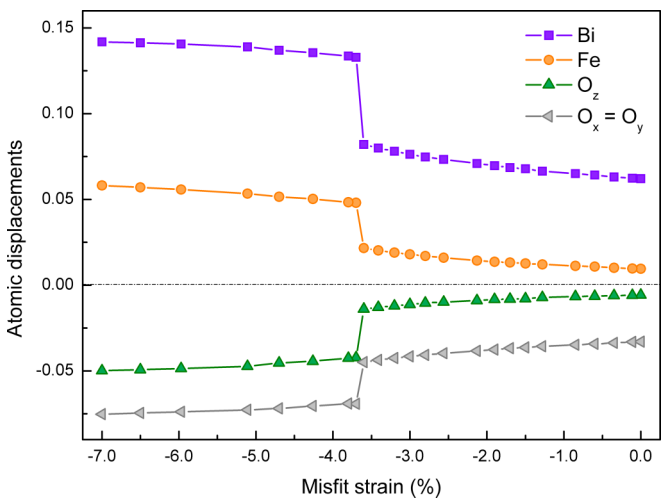


FIG. 4. Evolution of atomic displacements as a function of the epitaxial deformation at $T = 0$ K.

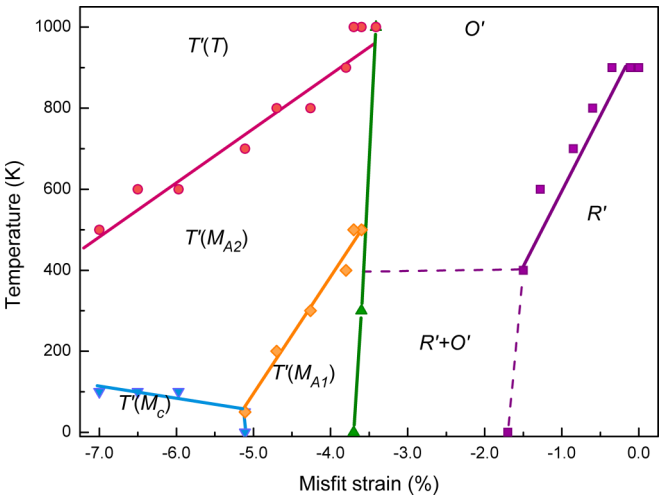


FIG. 5. Temperature-misfit strain phase diagram for $BiFeO_3$ obtained by the shell model simulations.

side) regions. Both regions are separated by a nearly vertical line, which represents the MPB.

At low strain levels in the $R$-like region, the temperature evolution resembles the behavior of the bulk. The simulations show that strained BFO undergoes a temperature-induced first-order transition from the $R'$ ($R3c$-like) phase to the $O'$ ($Pbnm$-like) phase. The transition is evidenced by the contraction of the out-of-plane lattice parameter, the absence of a net polarization ($P_x = P_y = P_z = 0$), and changes in the oxygen octahedra rotation pattern (Fig. 6). In this case, the rotation becomes in phase along $y$ direction ($\omega_y^M \neq 0$), while the out-of-phase order remains in the other two directions ($\omega_x^R \neq 0; \omega_z^R \neq 0$). The cell contraction at $T_C$ is in agreement with the experimental observations [12,13], although the model shows that the high-temperature phase is antiferroelectric rather than paraelectric. The phase displays antipolar $xz$ planes with polarizations along the $[101]_{pc}$ direction ($P_x^{AF}, 0, P_z^{AF}$) that is consistent with the $M_C$ type of monoclinic distortion suggested in Ref. [34]. Regarding the behavior of $T_C$ under strain, the simulation indicates that the transition temperature decreases with the application of strain, in agreement with experimental observations [12,13]. As shown in Fig. 1, the strain reduces the energy difference between $R'$ and $O'$, producing the downward shift in $T_C$. We note that the rate of change of $T_C$ is overestimated in comparison with experiments, and the transition temperature vanishes at $\varepsilon = -1.7\%$. As shown in Fig. 1, $R'$ and $O'$ phases have similar energies for $-3.7\% < \varepsilon < -1.7\%$. Both phases remain (meta)stable at finite temperature, and it is not possible to elucidate clearly the phase stability between them. This coexistence phase region is indicated in Fig. 5 by dotted lines.

The phases observed in the left region of the diagram are all ferroelectric with a strong polar component along the $z$ direction and a large tetragonal distortion. The two zero-temperature phases, $T'(M_{A1})$ and $T'(M_C)$, obtained as function of the epitaxial strain, display a first transition to a common $T'(M_{A2})$ phase. In this phase, $P_x = P_y < P_z$ and the oxygen octahedra do not rotate. The most noticeable feature of $T'(M_{A1}) - T'(M_{A2})$ transition is the change in

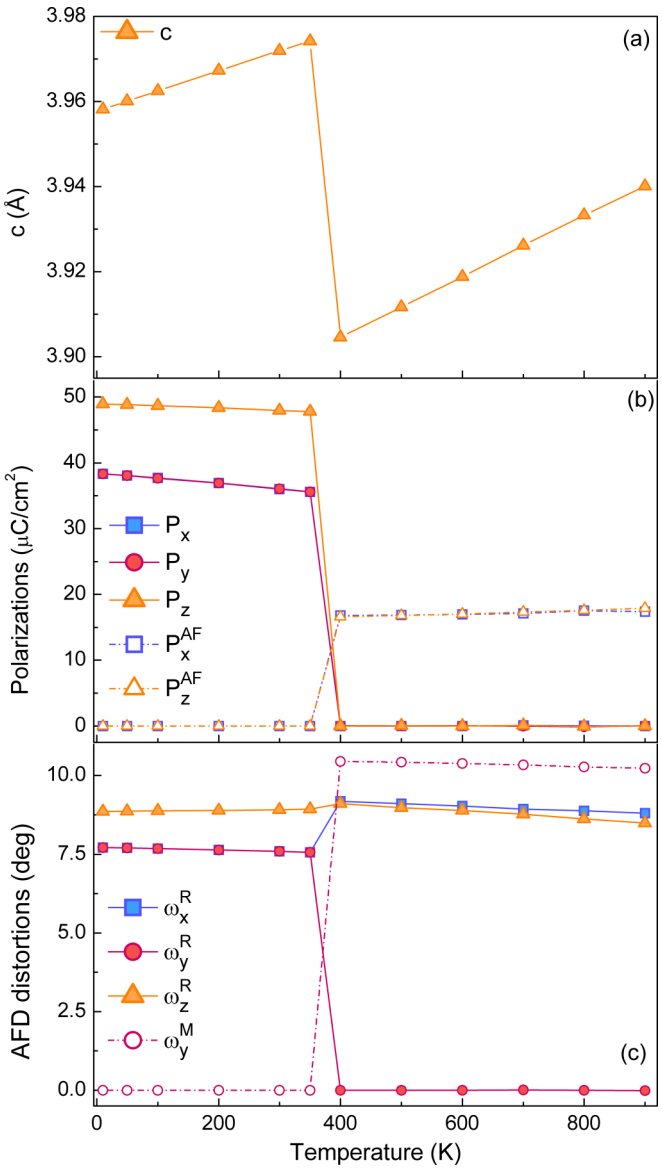


FIG. 6. Evolution of (a) $c$-lattice parameter, (b) FE and AFE polarizations, and (c) oxygen-octahedron rotation angles as a functions of temperature for $\varepsilon = -1.5\%$.

the oxygen rotational pattern, which completely disappears above the transition (see Fig. 7). In addition, there is a subtle change in the slope of the out-of-plane lattice parameter, while $\boldsymbol{P}$ is barely affected. The transition temperature to the $T'(M_{A2})$ phase decreases as strain increases. On the other hand, the $T'(M_C) - T'(M_{A2})$ transition is related with the local polarization pattern in the $xy$ plane. The domains pattern of the $T'(M_C)$ [see Fig. 3(b)] disappear at the transition, and local polarizations are all pointing along the same direction in the $T'(M_{A2})$ phase. Changes in the total polarization and lattice constant are not detected at the transition. Neither of the $T'(M_C)$ and $T'(M_{A2})$ phases displays rotation of the oxygen octahedra, and the temperature transition is practically independent of the strain. When the temperature increases, the $T'(M_{A2})$ displays a transition to a true tetragonal phase $T'(T)$ where the in-plane polar components vanish

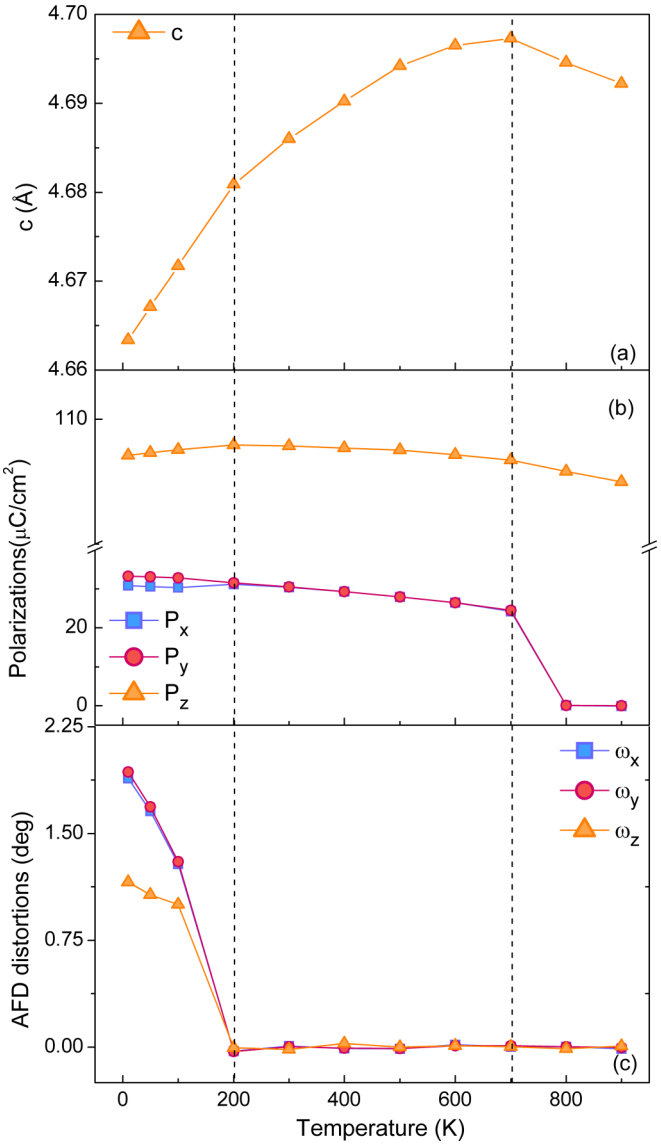


FIG. 7. Evolution of (a) $c$-lattice parameter, (b) polarizations, and (c) oxygen-octahedron rotation angles as functions of temperature for $\varepsilon = -4.7\%$.

($P_x = P_y = 0, P_z > 0$). The strain favors the stability of $T'(T)$ phase producing the reduction of the $T'(M_{A2}) - T'(T)$ transition temperature. The four different phases obtained in the $T$ region captures essential features experimentally observed in strained BFO films. In particular, the phase transition sequence $T'(M_C) - T'(M_A) - T'(T)$ as function of the temperature at high level of strains is in coincidence with the experimental reports in films deposited on $LaAlO_3$ and $YAlO_3$ substrates [35,36]. In addition, our description supports the presence of a second $M_A$ type of structure, which is stable at low temperatures near the MPB.

### C. The strain-induced MPB

The phase diagram of Fig. 5 shows different adjacent phases at the both sides of the MPB, offering the possibility of different strain-driven phase transitions. We first analyze the situation that represents the room temperature experimental observations, that is, $R'$ is the stable phase at the right side of the MPB. In this case the application of strain induces a $R' - T'(M_{A1})$ transition. We first note that the transition is isosymmetric and that it does not require changes in the polar and rotational order. Second, both phases are connected through a low energy barrier. Figure 1 shows that both structures are (meta)stable for strains near the MPB. We observe that the $R'$ phase loses its stability when compressive strains increase slightly above this critical region, and it naturally evolves to the $T'(M_{A1})$ structure. In a similar way, the $T'(M_{A1})$ structure becomes unstable for strain slightly below that region, and it goes into $R'$ structure. Finally, both structures are under opposite strain conditions in the MPB region. Figure 2(a) indicates that the $R'$ phase is under compression while $T'$ phase is under expansion. Therefore, simulation results are in concordance with the model for coexistence of phases proposed in Ref. [30]. Even more, the description is also consistent with the experimentally observed stability of the intermediate $S'$ phase [36,37], which can be described as an average of the $R'$ and $T'(M_{A1})$ phases.

A reversible transition between $R$ and $T$ regions occurs only at temperatures where $T'(M_{A1})$ is stable. We do not observe such a behavior at temperatures where the $T'(M_{A2})$ is stabilized. We attribute this fact to the different rotational order of the phases at both sides of the MPB. The change of the oxygen octahedral rotation patterns requires passing through higher energy barriers. This nonreversible behavior is also observed at higher temperatures for the $O' - T'(T)$ transition. This temperature-dependent behavior is consistent with the changes in the piezoelectric switching observed in highly strained film [36], and it highlights the relevance of the rotational degrees of freedom in the behavior of the compound across the MPB.

### D. Origin of the super tetragonal phase

To gain insight into the physical origin of the strain-induced tetragonal phase in BFO, we explore the behavior of the compound under hydrostatic pressure. Figure 8 displays the results for the enthalpy $H = E + P(V - V_0)$ as function of the pressure $P$, where $E$ and $V$ correspond to the energy and the volume of the particular structure and $V_0$ is the volume of ground state. The model displays a pressure induced transition from the ferroelectric $R3c$ phase to the orthorhombic $Pbnm$ structure. The transition pressure of 1.3 GPa is slightly underestimated with respect to the LDA value of 2 GPa [16]. In addition, our simulations show that a negative pressure of $-1.27$ GPa stabilizes a monoclinic $M_A$ phase with space group symmetry $Cm$. This tetragonally distorted phase displays a $c/a = 1.31$ and a volume increment of $\sim$7.6% at the transition phase. The polarization of the phases is $P_x = P_y = 28.7\,\mu C\,cm^{-2}$ and $P_z = 118\,\mu C\,cm^{-2}$, while oxygen octahedra are not rotated. The presence in BFO of a supertetragonal phase induced by strain or under negative pressure has similar characteristics to those seen in other perovskites, such as $PbTiO_3$ or $BaTiO_3$ [38,39]. In all cases, the $T'$ phase was achieved by an effective elongation of the cell along $z$ direction, regardless of whether the effect is obtained by compressive in-plane strain (or stress), tensile stress along

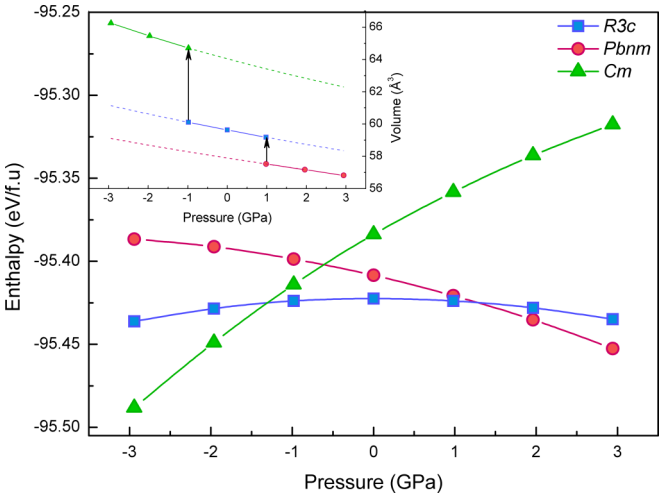


FIG. 8. Enthalpy $H$ of different metastable phases of $BiFeO_3$ under hydrostatic pressure as computed by the shell model.

$z$ direction or negative pressure. Then, our results support the hypothesis that the appearance of a highly elongated phase is a common feature of the ferroelectric perovskites. It was argued that the microscopic origin may be related to the breaking of bonds along the tetragonal axis. We want to stress that the shell model does not include electronic degrees of freedom explicitly; however, it is able to reproduce the strain-induced supertetragonal phase in agreement with experiments. The occurrence of the $T'$ phase with our model is not fortuitous. We verify that a model for $PbTiO_3$ [40] is also able to account the anomalous enhancement of the tetragonality reported from first-principles calculations [38].

## IV. CONCLUSIONS

The behavior of BFO under epitaxial strain has been explored with a first-principles based atomistic model. We find that the interatomic potential developed for the bulk is able to account for the marked structural changes that occurs at the strain-induced $R' - T'$ transition. The simulated phase diagram shows that the MPB is nearly independent of the temperature and displays the main phases experimentally observed in strained BFO films as function of the temperature. The paper reveals that order parameters related to the polarization and the rotation of the oxygen octahedra are required to describe such a complex the phase diagram. Finally, the induced supertetragonal phase in BFO is analogous to that observed in other perovskites, supporting the common origin of them.

## ACKNOWLEDGMENTS

We acknowledge computing time at the CCT-Rosario Computational Center. The paper was sponsored by Consejo Nacional de Investigaciones Científicas y Técnicas (CONICET), Grant No. PICT 2013-0423, Agencia Nacional de Promoción Científica y Tecnológica (ANPCyT), Grant No. PIP 2012- 0553, and Universidad Nacional de Rosario, Grant No. ING-376.

[1] W. Eerenstein, N. D. Mathur, and J. F. Scott, Nature **442**, 759 (2006).
[2] J. B. Neaton, C. Ederer, U. V. Waghmare, N. A. Spaldin, and K. M. Rabe, Phys. Rev. B **71**, 014113 (2005).
[3] G. Catalan and J. F. Scott, Adv. Mater. **21**, 2463 (2009).
[4] G. L. Yuan, S. W. Or, Y. P. Wang, Z. G. Liu, and J. M. Liu, Solid State Commun. **138**, 76 (2006).
[5] Z. Dai and Y. Akishige, J. Phys. D. Appl. Phys. **43**, 445403 (2010).
[6] T. Rojac, A. Bencan, G. Drazic, M. Kosec, and D. Damjanovic, J. Appl. Phys. **112**, 064114 (2012).
[7] M. Graf, M. Sepliarsky, R. Machado, and M. G. Stachiotti, Solid State Commun. **218**, 10 (2015).
[8] S. Fujino, M. Murakami, V. Anbusathaiah, S.-H. Lim, V. Nagarajan, C. J. Fennie, M. Wuttig, L. Salamanca-Riba, and I. Takeuchi, Appl. Phys. Lett. **92**, 202904 (2008).
[9] D. Kan, L. Pálová, V. Anbusathaiah, C. J. Cheng, S. Fujino, V. Nagarajan, K. M. Rabe, and I. Takeuchi, Adv. Funct. Mater. **20**, 1108 (2010).
[10] R. J. Zeches, M. D. Rossell, J. X. Zhang, A. J. Hatt, Q. He, C.-H. Yang, A. Kumar, C. H. Wang, A. Melville, C. Adamo, G. Sheng, Y.-H. Chu, J. F. Ihlefeld, R. Erni, C. Ederer, V. Gopalan, L. Q. Chen, D. G. Schlom, N. A. Spaldin, L. W. Martin, and R. Ramesh, Science **326**, 977 (2009).
[11] R. Ramesh and N. a Spaldin, Nat. Mater. **6**, 21 (2007).
[12] H. Toupet, F. Le Marrec, C. Lichtensteiger, B. Dkhil, and M. G. Karkut, Phys. Rev. B **81**, 140101 (2010).
[13] I. C. Infante, S. Lisenkov, B. Dupé, M. Bibes, S. Fusil, E. Jacquet, G. Geneste, S. Petit, A. Courtial, J. Juraszek, L. Bellaiche, A. Barthélémy, and B. Dkhil, Phys. Rev. Lett. **105**, 057601 (2010).
[14] D. Sando, B. Xu, L. Bellaiche, and V. Nagarajan, Appl. Phys. Rev. **3**, 011106 (2016).
[15] P. Ravindran, R. Vidya, A. Kjekshus, H. Fjellvåg, and O. Eriksson, Phys. Rev. B **74**, 224412 (2006).
[16] O. Diéguez, O. E. González-Vázquez, J. Wojdeł, and J. Íñiguez, Phys. Rev. B **83**, 094105 (2011).
[17] F. Kubel and H. Schmid, Acta Crystallogr. Sect. B Struct. Sci. **46**, 698 (1990).
[18] D. C. Arnold, K. S. Knight, F. D. Morrison, and P. Lightfoot, Phys. Rev. Lett. **102**, 027602 (2009).
[19] R. Haumont, I. A. Kornev, S. Lisenkov, L. Bellaiche, J. Kreisel, and B. Dkhil, Phys. Rev. B **78**, 134108 (2008).
[20] Y.-M. Kim, A. Kumar, A. Hatt, A. N. Morozovska, A. Tselev, M. D. Biegalski, I. Ivanov, E. A. Eliseev, S. J. Pennycook, J. M. Rondinelli, S. V Kalinin, and A. Y. Borisevich, Adv. Mater. **25**, 2497 (2013).

[21] M. Graf, M. Sepliarsky, S. Tinte, and M. G. Stachiotti, Phys. Rev. B **90**, 184108 (2014).
[22] M. Sepliarsky, A. Asthagiri, S. R. Phillpot, M. G. Stachiotti, and R. L. Migoni, Curr. Opin. Solid State Mater. Sci. **9**, 107 (2005).
[23] R. Machado, M. Sepliarsky, and M. G. Stachiotti, J. Mater. Sci. **45**, 4912 (2010).
[24] M. Sepliarsky and R. E. Cohen, J. Phys. Condens. Matter **23**, 435902 (2011).
[25] R. Machado, M. Sepliarsky, and M. G. Stachiotti, Appl. Phys. Lett. **103**, 242901 (2013).
[26] I. T. Todorov, W. Smith, K. Trachenko, and M. T. Dove, J. Mater. Chem. **16**, 1911 (2006).
[27] C. Ederer and N. A. Spaldin, Phys. Rev. Lett. **95**, 257601 (2005).
[28] D. H. Kim, H. N. Lee, M. D. Biegalski, and H. M. Christen, Appl. Phys. Lett. **92**, 012911 (2008).
[29] R. Haumont, P. Bouvier, A. Pashkin, K. Rabia, S. Frank, B. Dkhil, W. A. Crichton, C. A. Kuntscher, and J. Kreisel, Phys. Rev. B **79**, 184110 (2009).
[30] A. J. Hatt, N. A. Spaldin, and C. Ederer, Phys. Rev. B **81**, 054109 (2010).
[31] B. Dupé, I. C. Infante, G. Geneste, P.-E. Janolin, M. Bibes, A. Barthélémy, S. Lisenkov, L. Bellaiche, S. Ravy, and B. Dkhil, Phys. Rev. B **81**, 144128 (2010).
[32] Z. Luo, Z. Chen, Y. Yang, H.-J. Liu, C. Huang, H. Huang, H. Wang, M.-M. Yang, C. Hu, G. Pan, W. Wen, X. Li, Q. He, T. Sritharan, Y.-H. Chu, L. Chen, and C. Gao, Phys. Rev. B **88**, 064103 (2013).
[33] M. D. Rossell, R. Erni, M. P. Prange, J.-C. Idrobo, W. Luo, R. J. Zeches, S. T. Pantelides, and R. Ramesh, Phys. Rev. Lett. **108**, 047601 (2012).
[34] W. Siemons, C. Beekman, G. J. MacDougall, J. L. Zarestky, S. E. Nagler, and H. M. Christen, J. Phys. D. Appl. Phys. **47**, 034011 (2014).
[35] H.-J. Liu, H.-J. Chen, W.-I. Liang, C.-W. Liang, H.-Y. Lee, S.-J. Lin, and Y.-H. Chu, J. Appl. Phys. **112**, 052002 (2012).
[36] C. Beekman, W. Siemons, T. Z. Ward, M. Chi, J. Howe, M. D. Biegalski, N. Balke, P. Maksymovych, A. K. Farrar, J. B. Romero, P. Gao, X. Q. Pan, D. A. Tenne, and H. M. Christen, Adv. Mater. **25**, 5561 (2013).
[37] Z. Chen, Z. Luo, C. Huang, Y. Qi, P. Yang, L. You, C. Hu, T. Wu, J. Wang, C. Gao, T. Sritharan, and L. Chen, Adv. Funct. Mater. **21**, 133 (2011).
[38] S. Tinte, K. M. Rabe, and D. Vanderbilt, Phys. Rev. B **68**, 144105 (2003).
[39] H. Sharma, J. Kreisel, and P. Ghosez, Phys. Rev. B **90**, 214102 (2014).
[40] M. Sepliarsky, Z. Wu, A. Asthagiri, and R. E. Cohen, Ferroelectrics **301**, 55 (2004).